Arabian Journal of Chemistry (2020) **13**, 4065–4081

King Saud University

Arabian Journal of Chemistry

www.ksu.edu.sa
www.sciencedirect.com

ORIGINAL ARTICLE

A novel electrochemical sensor for determination of hydroquinone in water using $FeWO_4/SnO_2$ nanocomposite immobilized modified glassy carbon electrode

A. Karthika [a], V. Ramasamy Raja [b], P. Karuppasamy [e], A. Suganthi [a,c,*], M. Rajarajan [d,*]

[a] *PG & Research Department of Chemistry, Thiagarajar College, Madurai 625009, Tamil Nadu, India*
[b] *Department of Chemistry, K.P. National College of Arts and Science, Batlagundu 624202, Tamil Nadu, India*
[c] *Mother Teresa Women's University, Kodaikanal 624 102, Tamil Nadu, India*
[d] *Madurai Kamaraj University, Madurai 625 02, Tamil Nadu, India*
[e] *Anna University, Tirunelveli 627006, Tamil Nadu, India*

Received 14 February 2019; accepted 16 June 2019
Available online 22 June 2019

KEYWORDS

Electrochemical methods;
Anti-interference;
Amperometric method;
HQ sensor

Abstract A novel electrochemical sensor based on iron tungstate doped tin oxide nanocomposite Nafion ($FeWO_4/SnO_2$/Nf) immobilized modified glassy carbon electrode (GCE) is fabricated to determine hydroquinone (HQ) in this present study. The structural morphology and phase of $FeWO_4/SnO_2$ nanocomposite are characterized by X-ray powder diffraction (XRD), energy dispersive X-ray analysis (EDX), Fourier transform infrared spectroscopy (FT-IR), high transmission electron microscopy (HR-TEM) and Field emission scanning electron microscopy (FE-SEM), Brunauer-Emmett-Teller (BET) and X-ray photoelectron spectroscopy (XPS) respectively. Electrochemical methods such as cyclic voltammetry (CV), difference pulse voltammetry (DPV) and amperometric (i-t curve) are used to describe the electrochemical performance of the surface modified electrode for HQ sensing studies. The $FeWO_4/SnO_2$/Nf immobilized GCE is exhibited excellent catalytic activity with the increasing current signal during HQ sensing. The linear range of response is obtained between 0.01 μM and 50 μM for HQ detection under optimized conditions and the low detection limit (LOD) is found to be 0.0013 μM. Moreover, the present modified electrode shows

* Corresponding authors at: Mother Teresa Women's University, Kodaikanal (A. Suganthi).
E-mail addresses: suganthiphd09@gmail.com (A. Suganthi), rajarajanchem1962@gmail.com (M. Rajarajan).
Peer review under responsibility of King Saud University.

Production and hosting by Elsevier

https://doi.org/10.1016/j.arabjc.2019.06.008
1878-5352 © 2019 Production and hosting by Elsevier B.V. on behalf of King Saud University.
This is an open access article under the CC BY-NC-ND license (http://creativecommons.org/licenses/by-nc-nd/4.0/).

good reproducibility and excellent anti-interference behavior. In addition, the present electrochemical sensor is applied to the real samples of collected waters from various sources and the obtained experimental results are quite satisfactory.

© 2019 Production and hosting by Elsevier B.V. on behalf of King Saud University. This is an open access article under the CC BY-NC-ND license (http://creativecommons.org/licenses/by-nc-nd/4.0/).

1. Introduction

Hydroquinone (HQ) is an aromatic primary alcoholic derivative and also a hazardous material which generally affects the human health and ecological system. The major functions of dye synthesis, coal-tar production, photographic developers, paper manufacturing and cosmetics, etc. (Li et al., 2011). The increase of HQ absorption may affect the body and it creates a headache, fatigue, kidney damage and cancer (Ahammad et al., 2011). The HQ is considered as the critical ecological contaminant due to their abasement-resistant properties in the ecological environment system (Liu et al., 2014). It is toxic for the aquatic, ecological system even by low concentration, while the recent reports of European Union country (EU) and the United States (US) environmental protection organization (EPO) survey of aquatic environment pollutant shows a clear picture of HQ absorption in the environment (Xie et al., 2006). Contamination of HQ in the aquatic environment must affect the ecological system; hence this is a need of an hour to identify a solution. Recently different analytical methods are reported for the HQ detection included high-performance liquid chromatography (HPLC) (Marrubini et al., 2005), fluorescence (Pistonsei et al., 2006), chemiluminescence (Cui et al., 2006), pH based on flow injection, solid phase extraction method (Garcia-Mesa et al., 2007; Kova'cs et al., 2011) and pulse radiolysis (Mishra et al., 2008). The aforesaid methods are usually established at complicated laboratories, expensive instruments with highly qualified persons to operate and limited application for the real-time analysis. Apart from those expensive techniques, electrochemically sensing techniques are one of the simple, facile and accurate methods for the determination of HQ in aqueous media. Moreover, HQ oxidation is feasible to its hydroxyl group of benzene ring hard and also the detection of phenolic compounds directly by using bare electrodes does not show a clear redox peak. In recent years, the nanocomposite modified electrodes show better sensitivity and selectivity towards the sensing of HQ in aqueous media (Hu et al., 2012; Zhou et al., 2015). The method of sonochemical amalgamation could offer straightforward, cost-effective and evade high temperature and weight, the resultant particles are of uniform morphology, thin size, great crystallinity, and high virtue because of its prevalent acoustic cavitations force. Ultrasonication method used for 5000 K elevated temperature and 1000 atm pressure and 1010 K/s heating and cooling rate. This supports chemical reaction in good condition which produces a nanomaterial with high properties. Now a day, the semiconducting material-based nanocomposite is easily synthesized with the good active surface area by a sonochemical method in a short span of time (Selvarajan et al., 2018a, 2018b). As one of the large part of significant nanomaterials, tungsten oxides and other transition metal oxides was studied (Solis et al., 2001), widely used in solar cells (Mattioli et al., 2012), Li-ion batteries (Wu et al., 2012), photocatalysis (Vignesh et al., 2014), supercapacitors (Lang et al., 2011) and especially in electrochemical sensor (Jiang and Du, 2014) due to unique properties, such as high conductivity, catalytic activity and electrochemical sensitivity (Fukai et al., 2007; Jiang et al., 2014). Semiconductor metal oxides (MOx) nanostructures owning restricted and superior functional properties due to their crystallographic structures, predominantly SnO_2 is one of the promising compounds with large band gap and catalytic properties, hence it plays a remarkable role in sensor applications (Ingo et al., 2015). Though the metal oxide surfaces have great efficiency in determining binding affinity with adsorbates and charge transport between analyte and electrode, it indeed has to be enhanced by surface modifications to promote their sensitivity and selectivity. Additionally, for metal tungstate it is our focus on intensive research due to their high potential application in different fields such as photoluminescence, optical fibers, scintillator materials, humidity sensor, magnetic properties and catalysis (Zhang et al., 2007; Amano et al., 2008; Guo et al., 2010; Dai et al., 2010). The important derivative of $FeWO_4$ has been proven to display significant magnetic and optical properties (Hu et al., 2008; Zhou et al., 2009). Recently reported low-dimensional (quasi zero-dimensional or 1-D) synthesized metal tungstates including $MnWO_4$, Bi_2WO_6, $CdWO_4$, and $FeWO_4$ (Yu et al., 2003; Kloprogge et al., 2004) shows better electrochemical properties. Semiconducting metal oxides based nanocomposite plays an extraordinary role in the application of sensors due to their superior functional properties, charge transport, good catalytic, binding affinity between electrode and electrolyte to enhance the surface modification to support their better sensitivity and selectivity (Solis et al., 2001; Wu et al., 2012; Lang et al., 2011; Jiang et al., 2014; Fukai et al., 2007; Yu et al., 2003).

The present work aims to fabricate a semiconducting material-based nanocomposite modified ($FeWO_4/SnO_2$/Nf) immobilized GC electrode for selective and sensitive determination of HQ in different water samples. The prepared $FeWO_4/SnO_2$ nanocomposite is characterized by several spectroscopic (FT-IR, XRD, BET, XPS FE-SEM, EDX, HR-TEM, SEAD, and Mapping analysis) and electrochemical (cyclic voltammetry (CV), differential pulse voltammetry (DPV) and amperometric (i-t curve)) techniques. Herein, we have used Nafion (Nf) for immobilization of $FeWO_4/SnO_2$ nanocomposite material on the surface of the GC electrode. Nafion (Nf), a perfluorosulfonated ion-exchange polymer and has a good advantage to act as electrode modifier in the field of electrocatalysis in the past three decades (Ganesan et al., 2001; Ganesan and Ramaraj, 2001; Azad and Ganesan, 2010a, 2010b). The immobilization of catalytic molecules on electrode surface has the advantages over the bare electrodes as (i) modified electrodes alter the overall rate of electrochemical reactions, (ii) the catalyst is readily separated from the solution medium and (iii) a very small amount of catalyst is required for the electrocatalytic reactions (Ciucu, 2014). The electrode modification allows the electrocatalyst to be dispersed at the molecular level with good activity towards many electrocatalytic reactions (Turdean et al., 2006; Almeida et al., 2007; Umar et al., 2008; Rahman and Asiria, 2015; Awual et al., 2016). The present experimental data clearly indicated that the present modified nanocomposite ($FeWO_4/SnO_2$/Nf) immobilized GC electrode has better sensitivity, selectivity, low detection limit and good catalytic recovery for the HQ detection in different water samples are collected from tap, river and lake resources.

2. Experimental section

2.1. Materials and methods

Hydroquinone, resorcinol, catechol, neurotransmitters, serotonin, dopamine, uric acid, cystine, norepinephrine, ascorbic acid, and glucose were purchased from Merck chemicals company. Sodium tungstate, stannous chloride pentahydrate, iron chloride, and sodium hydroxide were obtained from Sigma-Aldrich and used as such. The stock solution and electrolyte solutions were prepared using deionized water without any further purification. The pH = 7.0 (Phosphate buffer saline

(PBS)) was prepared by using the appropriate ratio of 0.1 M (1 g) sodium dihydrogen phosphate and (2 g) disodium hydrogen phosphate dissolved in water and the pH range was adjusted by using 0.1 M orthophosphoric acid and 0.1 M NaOH solution.

The surface morphology and particle size of $FeWO_4/SnO_2$ were determined by FE-SEM through a Carl Zeiss, Germany (Supra 35-VP) operated at 15 kV and HR-TEM (model: T20 -G2, Fei Tecnai, USA) techniques. The FT-IR spectra were performed using FT-IR spectrophotometer (model: 460Plus, JASCO, Japan) by KBr Pellet making method. A Kratos Axis Ultra X-ray photoelectron spectroscopy (Al Kα source) was employed to record the XPS spectra. Nitrogen adsorption-desorption isotherms were measured at 77 K with micrometritics ASAP 2020 sorptometer. The crystalline phase, size, and structure of the $FeWO_4$, SnO_2 and $FeWO_4/SnO_2$ samples were detected by XRD 6000 (Hitachi, Japan), X-ray diffractometer with Cu-Kα radiation (λ = 0.154060 nm) at a scanning rate of 0.05° per second in the 2θ range from 20° to 80°. The specific surface area was calculated with the Brunauer-Emmett-Teller (BET) equation, and the pore size distribution was calculated from the adsorption curve by the Barrett–Joyner–Halenda (BJH) method. All electrochemical experiments were performed with CHI660E electrochemical Analyzer, USA. Conventional three-electrode system with a GCE (Ø = 3.0 mm) was used for fabrication of modified electrode as a working electrode, 0.1 M KCl saturated Ag/AgCl used as the reference electrode and a platinum wire used as the counter electrode. Before start electrochemical experiments, the electrolyte with high purity nitrogen gas was pre-purged for 10–15 min to oxygen remove and all the electrochemical experiments were performed at room temperature. The water samples were collected from the resources such as tap (lab), lake (Thekkady) and river (Mullai Periyar).

2.2. Synthesis for $FeWO_4$

$FeWO_4$ nanocomposite was synthesized from the mixture of 1.0 g of $Na_2WO_4{\cdot}2H_2O$ and 2 g of Fe $(NH_4)_2$ $(SO_4)_2{\cdot}6H_2O$ [1:2] dissolved in (100 ml) deionized water. The aforesaid mixture was stirred well for 25 min with 10 ml NaOH (0.2 M) solution was added slowly. The mixture was transferred into an autoclave (Teflon line stainless steel) and maintained the temperature at 180 °C for 6 h (Bhosale et al., 2019; Dadigala et al., 2019). The resulted precipitate was filtered using Whatman filter paper and the purification of precipitate was carried out by using ethanol and water. A black color precipitate was obtained dried at 60 °C for 12 h.

2.3. Synthesis for SnO_2

The starting material of 5 g $SnCl_4{\cdot}5H_2O$ (0.1 M) was dissolved in (50 ml) deionized water with constant stirring and then NaOH (0.2 M) [1:2] dropped wise added into above mixture solution at pH = 9 (Zhang et al., 2019). The mixture was transferred into Teflon lined stainless steel autoclave heated at 180 °C for 3 h. The resultant product was filtered using NO.1 Whatman paper with ethanol and water. A white color precipitate was obtained and that was dried at 180 °C for 4 h using drier.

2.4. Synthesis for $FeWO_4/SnO_2$

The $FeWO_4/SnO_2$ nanocomposite was synthesized from the mixture of (0.1 M) SnO_2 (2 g in 30 ml H_2O) with (0.5 M) $FeWO_4$ (4 g 30 ml H_2O) were mixed in a 100 ml beaker and allowed to stand ultrasonication bath for 2 h. Then the mixture solution was ultrasonicated for 180 min with slow addition of 2 ml conc. HCl into the solution. Afterward, the reaction mixture was transferred into 100 ml beaker and stirred it using magnetic stirrer for 24 h. Then, the resultant brown product was gently collected by centrifugation and washed thoroughly with ethanol and DI water for several times and dried at 80 °C for 12 h.

2.5. Fabrication of $FeWO_4/SnO_2$/Nf immobilized modified GC electrode

First the electrode modification, the mirror-like surface of GCE was polished with 0.03 μm and 0.05 μm alumina paste and a polish cloth. In the removal of the alumina residues on the GCE surface, the GC electrode was sonicated in 1:1 nitric acid, alcohol and deionized water for 10 min time interval and next allowed to dry at room temperature. With the aim of fixation of nanocomposite on GCE, 1 mg $FeWO_4/SnO_2$ nanocomposite and 5 ml of nafion are dispersed into the solution by ultra-sonication method for 30 min. After it is sonicated, 8 μL of $FeWO_4/SnO_2$/Nf dispersive solution is pipetted out and dropped onto the GCE surface and dried in oven for 40 min. After drying process, the modified GCE is softly rinsed with 5 ml of deionized water to remove the weakly bounded materials on GCE surface. Finally, obtaining nanocomposite modified GCE is used to sense HQ in the present study (Scheme 1).

3. Results and discussion

3.1. Characterization

Powder XRD analysis is employed for the further study of the composition of $FeWO_4/SnO_2$ nanocomposite and the result is shown by Fig. 1. It indicated three characteristic diffraction peaks of typical $FeWO_4$ sample indexed monoclinic phase (JCPDS number file No. 46-1446) through the lattice parameters of ca = 4.739 Å, b = 5.718 Å, c = 4.965 Å which corresponds to the (1 1 1), (2 0 0) and (2 2 0) crystal planes respectively (Zhang et al., 2007; Aslam et al., 2017; Hussain et al., 2017a, 2017b). The diffraction peak for pure SnO_2 with the phase of tetragonal (JCPDS-880287) is observed at 2θ = 18°, 30°, 31°, 36° and 70°. The well-defined diffraction peaks attributed that the samples at 2θ values of 32.8 nm (SnO_2), 15.83 nm ($FeWO_4$) and 21.36 nm ($FeWO_4/SnO_2$) are shown by Fig. 1, which corresponds to the (0 0 2), (1 0 0) and (1 0 0) crystal planes of $FeWO_4/SnO_2$ nanocomposite. The XRD results are authenticated that the successful preparation and fabrication of $FeWO_4/SnO_2$ nanocomposite. FT-IR spectra of $FeWO_4$, SnO_2, and $FeWO_4/SnO_2$ are shown in Fig. 2. Fig. 2a clearly indicated that the presence of Fe—O—W symmetrical vibrational peaks at 450 cm^{-1}, 834 cm^{-1} and 874 cm^{-1} respectively. The peaks at 633 and 710 cm^{-1} are assigned to the W—O stretching vibration, which may well

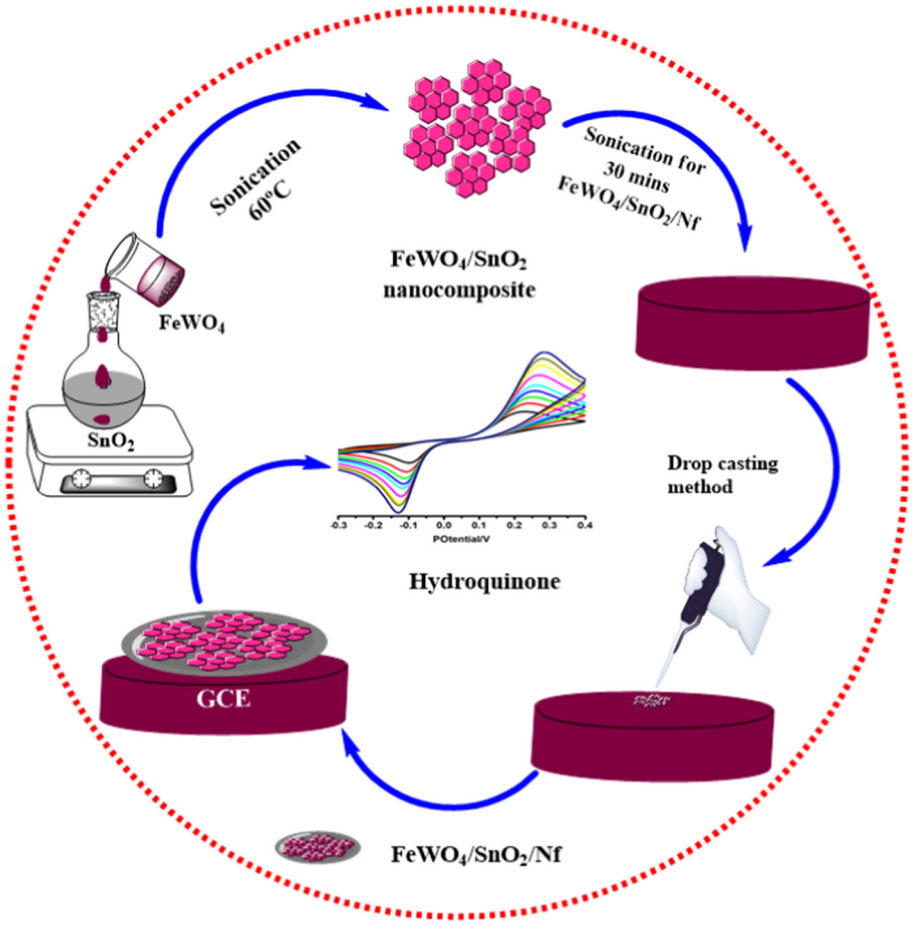

Scheme 1 Stepwise fabrication of $FeWO_4/SnO_2$/Nf immobilized modified GC electrode for HQ sensor.

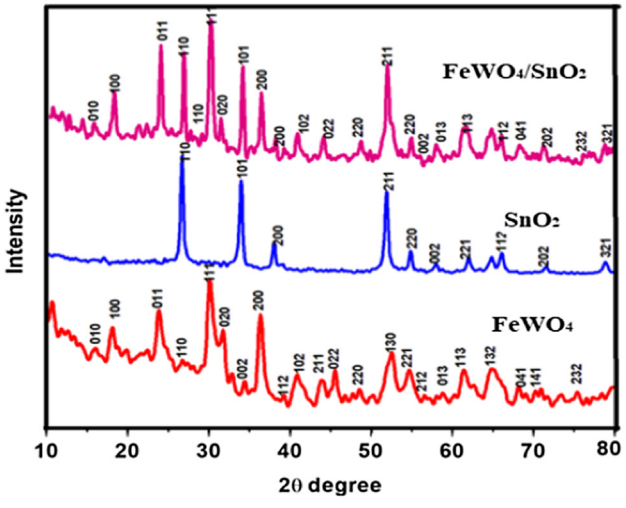

Fig. 1 XRD pattern of (a) $FeWO_4$, (b) SnO_2 and (c) $FeWO_4/SnO_2$ nanocomposite.

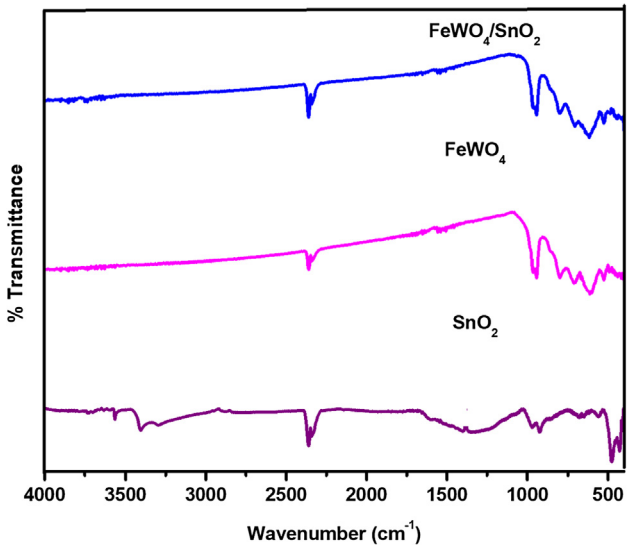

Fig. 2 FT-IR spectrum of (a) $FeWO_4$, (b) SnO_2 and (c) $FeWO_4/SnO_2$ nanocomposite.

be attributed to stretching vibration of O—H bond of water molecules, as well as another one at 1600 cm^{-1} assigned to angular vibration of water molecules (Perfecto et al., 2016; Jenita Rani et al., 2016). The Fe—O symmetric and asymmetric vibrational frequencies are observed at 473 and 532 cm^{-1} respectively (Amano et al., 2008; Guo et al., 2010; Dai et al., 2010; Zhou et al., 2009). Fig. 2b clearly shows the Sn—O stretching vibrational frequency is appeared below 600 cm^{-1}

and absorbed water on the surface of the sample and the peaks around 1000–1500 cm^{-1} correspond to stretching vibration of SnO_2 (Ingo et al., 2015). The main functional group present in curve c is confirmed the formation of (Fe—O—W, Fe—O, W—O, and Sn—O) $FeWO_4/SnO_2$ nanocomposite. All the FT-IR spectral data are in good agreement with the reported values (Saravanakumar and Muthuraj, 2017; Kloprogge et al., 2004). The pore structure of (a) $FeWO_4$, (b) SnO_2 and (c) $FeWO_4$ /SnO_2 composite have been investigated by the nitrogen adsorption–desorption experiment at −196 °C. The corresponding pore size distribution and specific surface area were determined using the BJH method and BET method respectively. The N_2 adsorption-desorption isotherm and pore size distribution curve were shown in Fig. 3. Fig. 3 displayed a typical character of type IV isothermal curves with a hysteresis loop appeared in the range of 0.3–0.8 (P/P_0), according to the IUPAC classification [30,31]. The surface area $S_{B.E.T}$ (m^2/g), pore volume (cm^3/g) and pore size (nm) were calculated using B.E.T equation and the results are listed in Table 1. The results indicate that the prepared nanocomposite is mesoporous in nature. The B.E.T surface area was found to be 38.58 m^2/g and 53.76 m^2/g, 33.01 m^2/g for (a) $FeWO_4$, (b) SnO_2 and (c) $FeWO_4$ /SnO_2 composite respectively. It is obvious from the figures that the surface areas and pore volumes of $FeWO_4$ are significantly increased when it was modified with SnO_2.

Table 1 N_2 adsorption-desorption isotherm and Barrett–Joyner–Halenda (BJH) pore size distribution of $FeWO_4/SnO_2$ nanocomposite.

Samples	Specific surface area (m^2/g)	Average pore diameter (nm)	Pore volume (cm^3/g)
SnO_2	33.01	11.32	0.3612
$FeWO_4$	38.58	19.39	0.4155
$FeWO_4$/ SnO_2	53.76	53.38	0.6359

The chemical composition and surface chemical states of the as-obtained $FeWO_4/SnO_2$ nanocomposite was investigated by XPS and the corresponding results are shown in Fig. 4. Fig. 4a shows the XPS spectrum of XPS of the synthesized $FeWO_4/SnO_2$ nanomaterial. The main peaks at 712.6, 35.6, 283.2, 496.8 and 527.8 eV can be attributed to the binding energies of Fe(2p), W(4f), C(1 s), Sn(3d) and O(1 s) respectively. The XPS spectrum shows the predominant carbon peak due to pump oil during the vacuum treatment before the XPS test. In the Fig. 4b, the XPS peak values at 483.2 and 494.6 eV were assigned $Sn3d_{3/2}$ and $Sn3d_{5/2}$ binding energies respectively. In Fig. 4c, shows two XPS peaks at 712.6 and 726.2 eV were assigned to $Fe2p_{3/2}$ and $Fe2p_{1/2}$ binding energies

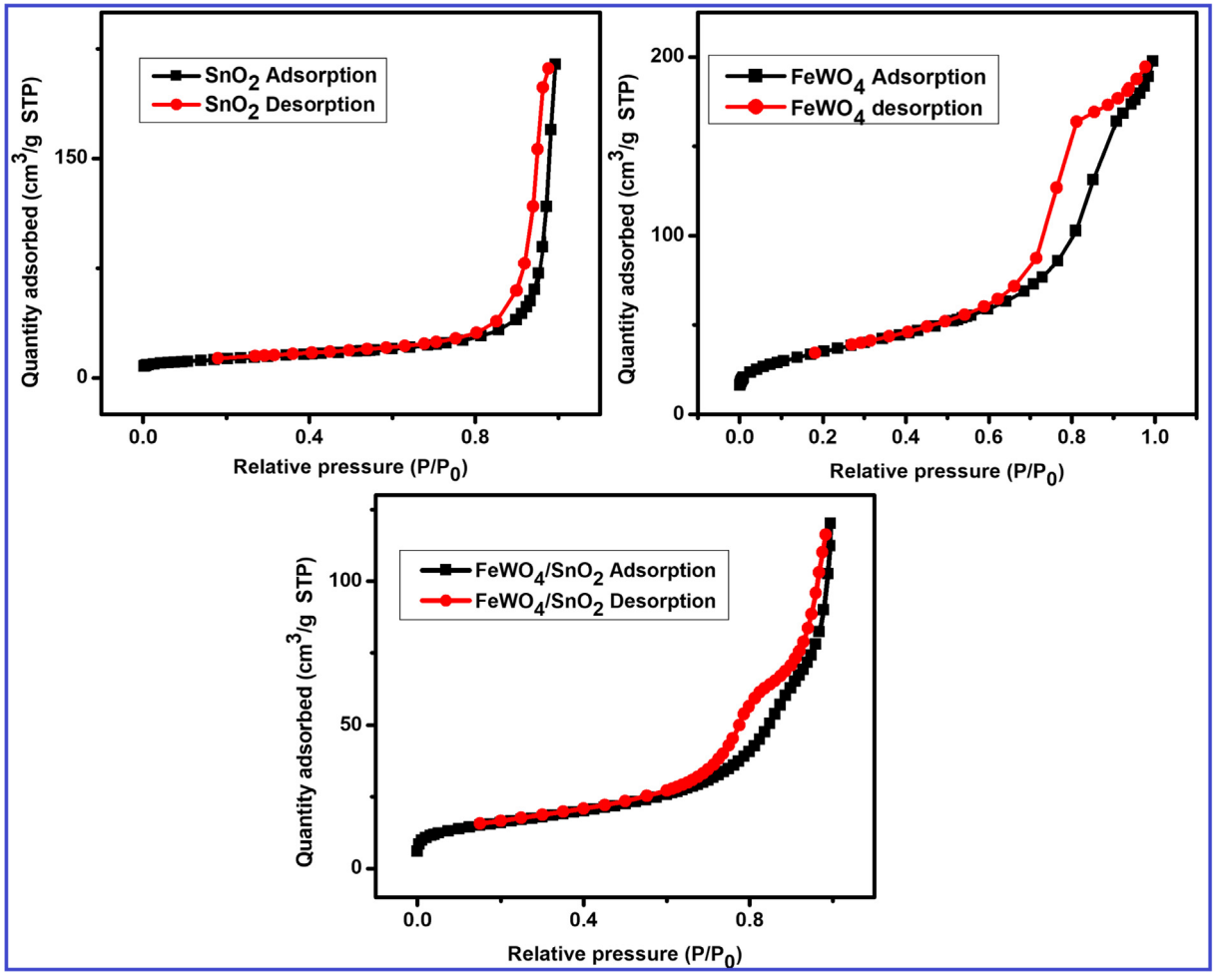

Fig. 3 Adsorption-desorption isotherm of (a) SnO_2, (b) $FeWO_4$ and (c) $FeWO_4/SnO_2$ nanocomposite.

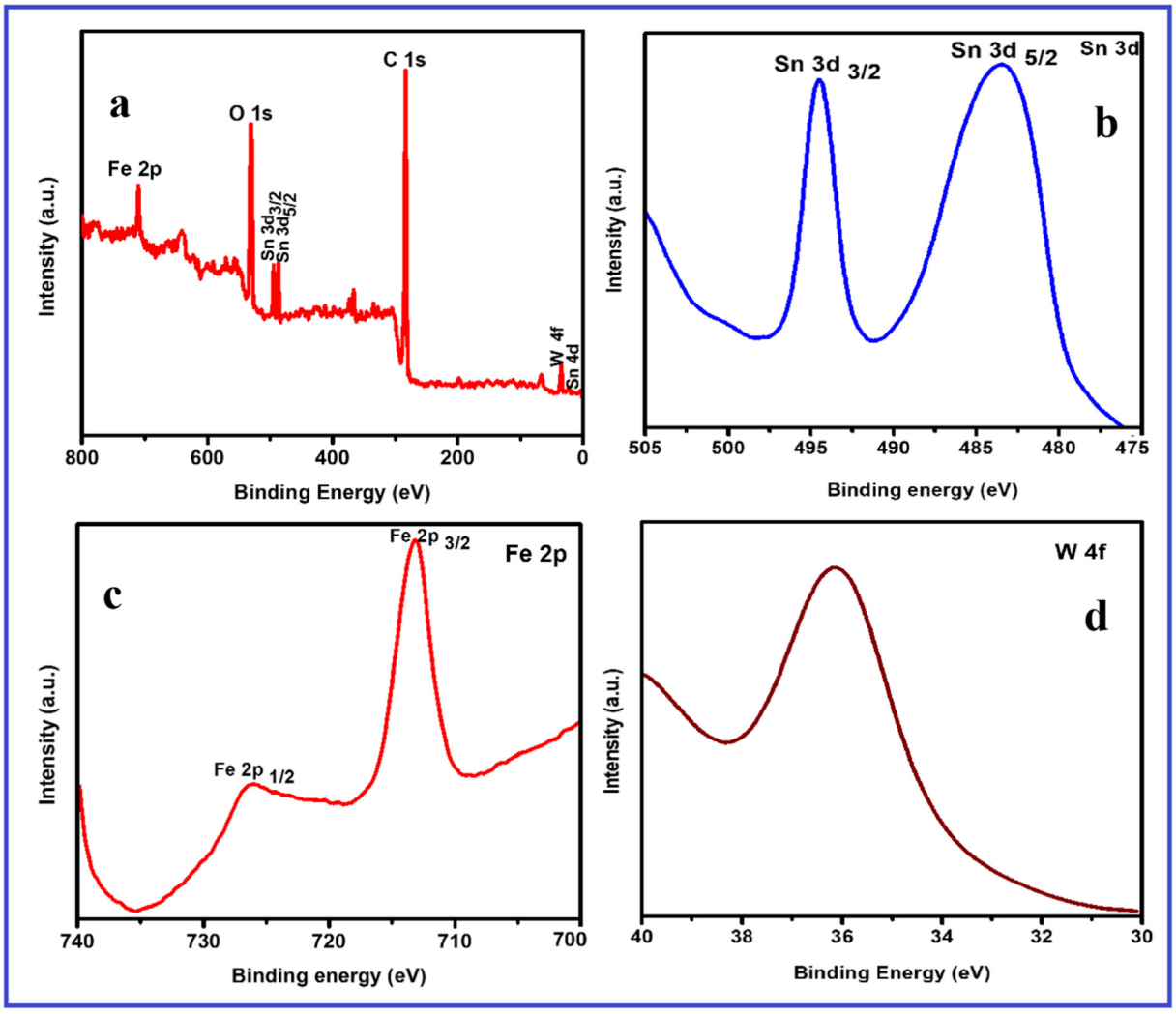

Fig. 4 XPS spectra of $FeWO_4$ /SnO_2 nanocomposite: (a) XPS survey scan; (b) Sn 3d spectrum; (c) Fe 2p spectrum; (d) W 4f spectrum.

respectively. The XPS peak value at 35.6 corresponds to tungsten (W4f) in the formal valence of +6.

The FE-SEM image of $FeWO_4$, SnO_2 and $FeWO_4/SnO_2$ are shown in Fig. 5. Fig. 5a, c and e are depicted that the FE-SEM images of the prepared $FeWO_4$, SnO_2 and $FeWO_4/SnO_2$ respectively. Fig. 5a and c, are showed the characteristic FE-SEM images of the smooth surface of $FeWO_4$ (nanorods shape) and SnO_2 (spherical shape) and it is randomly distributed. But Fig. 5e clearly indicates that the formation of the nanoflake structure of $FeWO_4/SnO_2$ nanocomposite. The prepared $FeWO_4/SnO_2$ nanocomposite by sonication method shows uniform surface and particle diameter respectively. The $FeWO_4/SnO_2$ provides larger surface area, better surface activity and efficient transmission channel for detection of analytes and helped to reach the active sites, to improve the sensitivity of the nanocomposite surface modified electrode (Awual et al., 2017a, 2017b). Fig. 5b, d, and f are showed the corresponding EDX spectrum of $FeWO_4$, SnO_2, and $FeWO_4/SnO_2$, which confirms the appearance of following elements such as Fe, W, O, and Sn. After the formation of the nanocomposite, the presence of the element in the nanocomposite is observed from the morphology changes by the EDX spectrum as shown in Fig. 5. The obtained EDX data are in good agreement with the reported nanocomposite EDX spectrum (Karthika et al., 2019). The unique morphology of $FeWO_4/SnO_2$ nanocomposite is confirmed by HR-TEM, as shown in Fig. 6a–d by different magnification. From Fig. 6e we confirm that the hexagonal plate shape occurred between of large size particles of $FeWO_4$ and nanosheets of SnO_2 to form the nanocomposite. Fig. 6f indicates that the crystalline nature of $FeWO_4/SnO_2$ nanocomposite is observed in the selected area of the electron diffraction pattern (SAED). The mapping of nanospheres of $FeWO_4/SnO_2$ composite is indicated that the presence of the element such as Fe, Sn, W, and O respectively as shown by Fig. 7a–f.

3.2. Electrochemical behaviour of HQ on the modified electrode

Electrochemical performance of $FeWO_4/SnO_2$/Nf immobilized modified GC electrode was characterized using a cyclic voltammetric method (Ribeiro et al., 2015; Rahman et al., 2017a, 2017b, 2017c, 2017d; Alam et al., 2017). The obtained CV is shown in Fig. 8 (a) bare GCE (black colour), (b) $FeWO_4$ (red colour), (c) SnO_2 (blue colour) and (d) $FeWO_4/SnO_2$/Nf

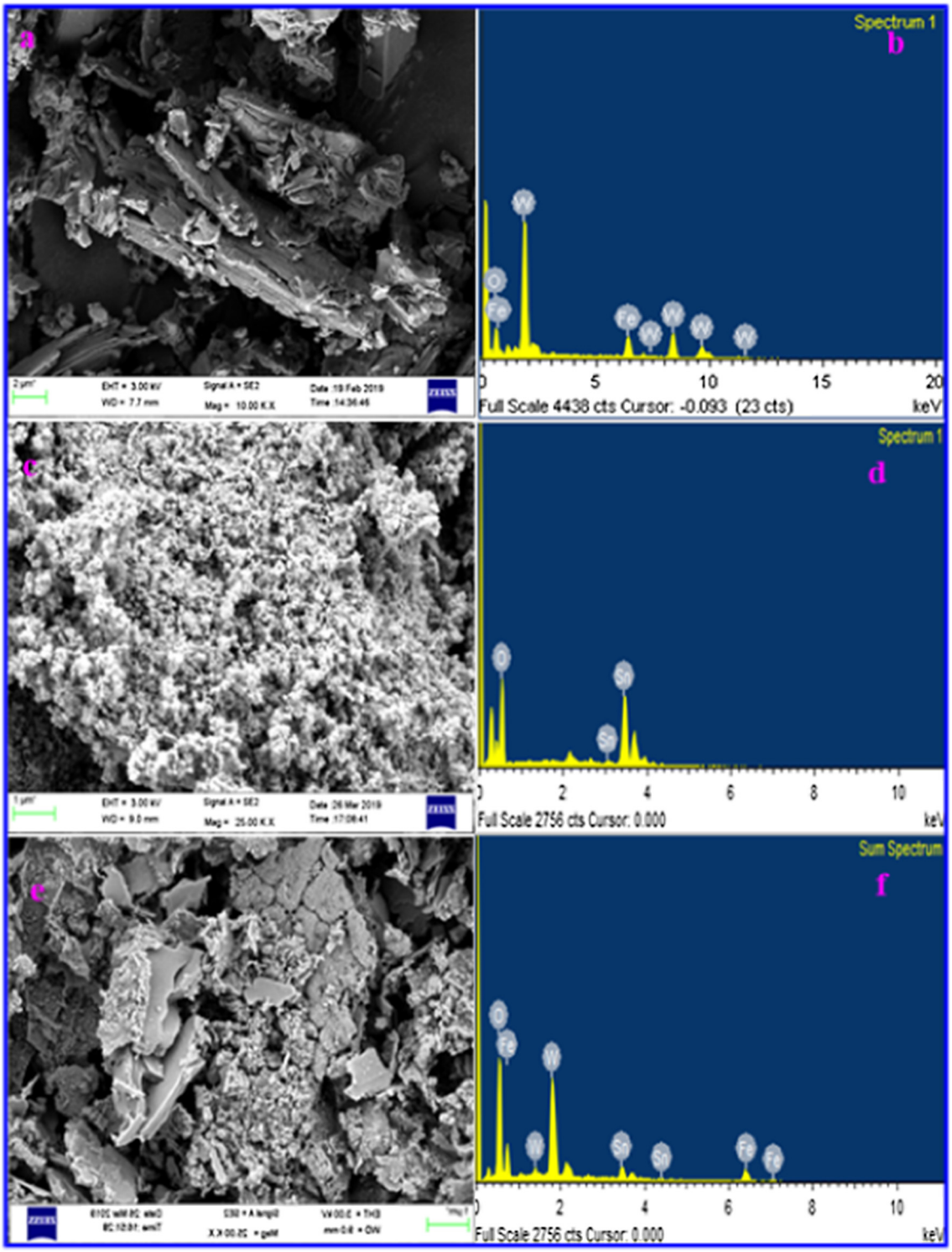

Fig. 5 FE-SEM image of (a) $FeWO_4$, (b) SnO_2 and (c) $FeWO_4$ /SnO_2 with EDAX image of (d) $FeWO_4$, (e) SnO_2 and (f) $FeWO_4$/SnO_2 nanocomposite.

(green colour) immobilized modified GC electrodes in 0.1 M PBS (pH = 7) containing 10 μM HQ, the potential range between −0.3 V and 0.4 V respectively. As shown in Fig. 8a there is no redox peak observed in the case of the bare GCE, which suggests that the redox peak of HQ is not detected separately at the bare GCE (Huan et al., 2004; Selvarajan et al., 2018a, 2018b; Ahmed et al., 2018). At the same time, in the presence of 10 μM HQ with $FeWO_4$/GCE, SnO_2/GCE and $FeWO_4$/SnO_2/Nf immobilized modified GCE well-defined anodic peak current at the potential of 0.140, 0.203 and 0.283 V, respectively as shown in Fig. 8. Moreover, $FeWO_4$/SnO_2/Nf immobilized modified GC electrode shows an

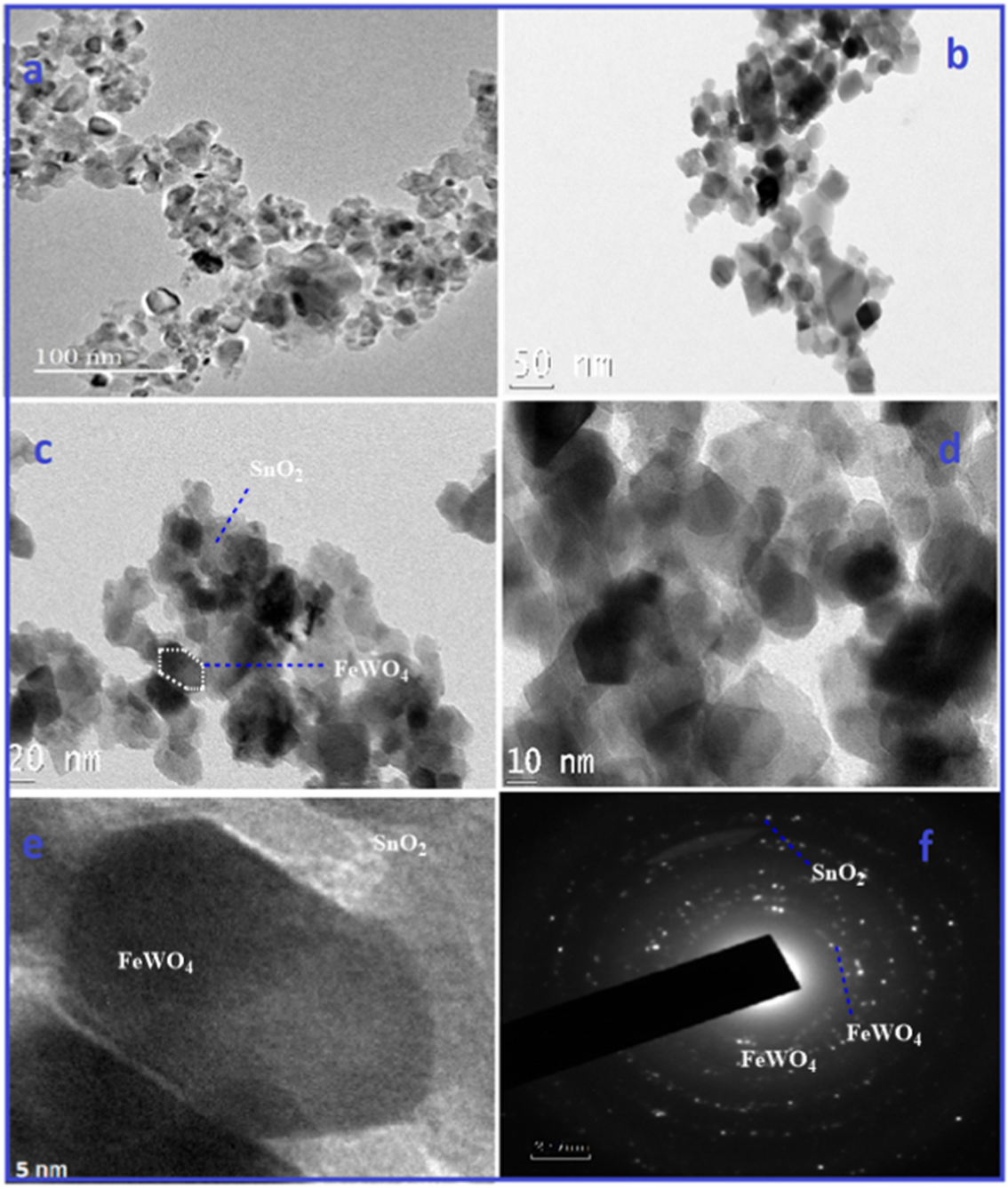

Fig. 6 HRTEM image and SAED pattern of $FeWO_4/SnO_2$ nanocomposite.

enhanced anodic peak current and lower peak potential when compared to bare GCE, $FeWO_4$ and SnO_2 modified GCEs as shown in Fig. 8b and c. This observation indicates that the presence of $FeWO_4$ and SnO_2 the electron transfer occurred to the electroactive molecules on the GCE surface. The CV obtained using $FeWO_4/SnO_2$/Nf immobilized modified GCE shows a dramatical increase of oxidation peak current, which also increases the adsorption onto HQ of the electrode surface, is shown in Fig. 9. Moreover, $FeWO_4/SnO_2$/Nf immobilized modified GCE could enhance the effective surface area for high electron transport, electrocatalytic activity, sensitivity for the detection of HQ.

3.3. Effect of scan rate

Fig. 10 revealed the scan rate on the current peak and potential peak of HQ and it is evaluated by cyclic voltammetry in 0.1 M PBS at pH = 7.0. The CV of HQ detection shows that the reduction and oxidation peak currents are linearly increasing with increasing scan rate in the linear range between 10 mV s^{-1} and 90 mV s^{-1} respectively. The plot of peak current vs. scan rate is found to be linear and the slope values are Ipa (μA) = 0.3519x + 1.3421 mV s^{-1} and correlation coefficient values are R^2 = 0.9963 respectively. The observed result reveals that the electrochemical HQ detection of $FeWO_4/SnO_2$/Nf immobi-

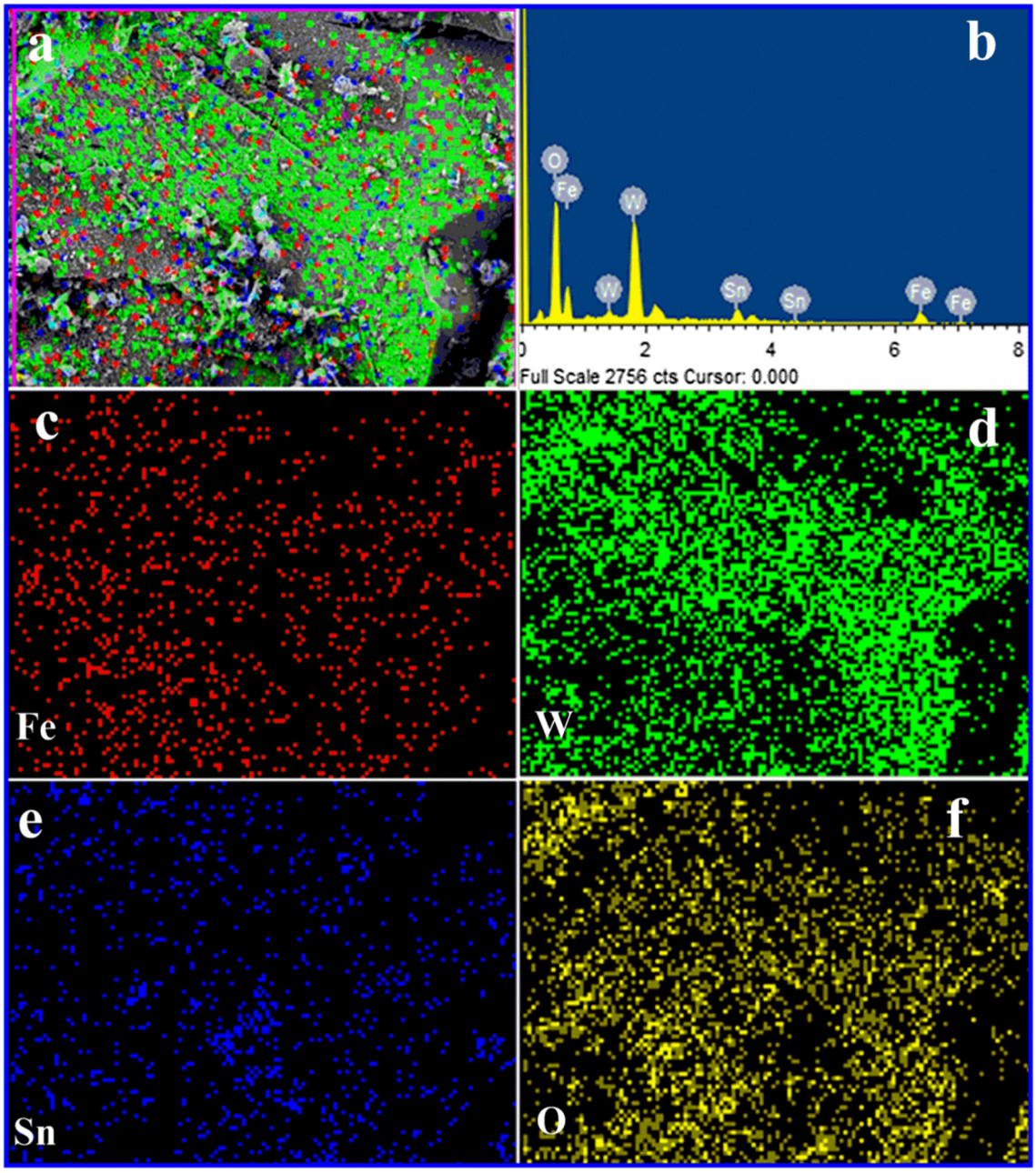

Fig. 7 Mapping analysis for FeWO4/SnO_2 nanocomposite.

lized modified GCE surface is a diffusion controlled process (Chen et al., 2017a, 2017b). The value of peak potential (Ep) of $FeWO_4/SnO_2$/Nf immobilized modified GCE is proportional to the logarithm of the scan rate log (υ). Electron transfer rate constant (Ks) and the charge transfer coefficient (α) of the analytes are determined using the following Eqs. (1) and (2) (Karim-Nezhad et al., 2017). The peak potentials (Epa) of $FeWO_4/SnO_2$/Nf immobilized modified GCE is directly proportional to the log of scan rate. The plot of peak potentials versus log of scan rate is linear as shown in Fig. 10c and correlation coefficient value (R^2) value is found to be 0.996. The electron transfer rate constant (Ks) and charge transfer coefficient are calculated from Eq. (1) (Laviron, 1979).

$$E_p = K - \frac{2.303RT}{\alpha nF}\log v \quad (1)$$

The calculated charge transfer coefficient is $\alpha = 0.49$ ($n = 2$) $FeWO_4/SnO_2$/Nf immobilized modified GCE.

$$\log k_s = \alpha\log(1-\alpha) + (1-\alpha)\log\alpha - \log\frac{RT}{nFv} - \frac{\alpha(1-\alpha)nFE}{2.303RT} \quad (2)$$

The calculated α-value is substituted to the Eq. (2), we can be determined the electron transfer rate constant "K_s" and "K_s" value is found to be $3.59 \pm 0.5\ s^{-1}$.

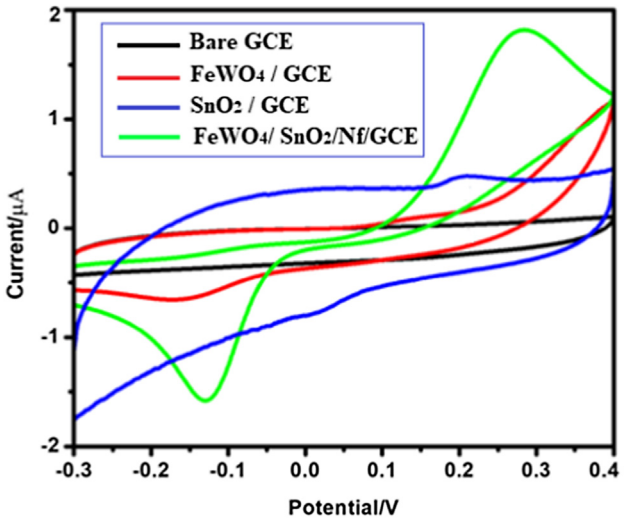

Fig. 8 Cyclic voltammetric response of (a) bare GCE (black colour), (b) $FeWO_4$ (red colour), (c) SnO_2 (blue colour) and (d) $FeWO_4/SnO_2$/Nf (green colour) immobilized modified GC electrodes in the presence of 10 μM HQ containing 0.1 M (pH = 7) PBS at a scan rate of 100 mV/s.

3.4. Effect of pH

The electrochemical behavior of HQ is carried out via CV and DPV in 0.1 M PBS with different pH range from 3.0 to 9.0 (Fig. 11). Generally pH of the electrolyte solution may be influenced the electrochemical sensitivity. The peak current is increased with increasing pH from 3.0 to 7.0 but pH is above7.0 the peak current decreases. Because HQ is a protic aromatic molecule (pK_a = 9.850), which can be easily generate deprotonation and turn to anions. At low pH range and it is protonated in the form of $-OH^{2+}$ (Yao et al., 2016) when increasing the pH from 3.0 to 7.0, thus the peak current increases, whereas pH > 7 hydroxyl ions are increased and it might be decreased the HQ adsorption in the solution onto the electrode surface so that the redox current decreased at pH > 7. Therefore, in order to achieve high sensitivity, pH = 7.0 has been chosen for determination of HQ in this present study (Zheng et al., 2013; Rahman, 2018; Hussain et al., 2017a, 2017b).

The plot between the redox peak potential and pH is linear as shown in Fig. 8b and obtained slope value (−59 mV/pH) is very close to the theoretical value of −59 mV/pH, which reveals that the number of electrons and protons are taking part in the electrochemical reaction is equal. Thus, the electrochemical oxidation of HQ at $FeWO_4/SnO_2$/Nf immobilized GCE should be a two-electron and two-proton transfer process (Chen et al., 2019). The possible electron transfer (ET) mechanism for determination of HQ using $FeWO_4/SnO_2$ nanocomposite immobilized GCE is presented in Scheme 2.

3.5. DPV

DPV is a versatile technique for determination of HQ and the obtained DPV for determination of HQ is shown in Fig. 12a. The increment of HQ concentration, the anodic peak current is increased (Lower–higher) using $FeWO_4/SnO_2$/Nf immobilized GCE (Arshad et al., 2017; Rahman et al., 2017a, 2017b, 2017c, 2017d). A well defined increased anodic peak potential is observed at the peak potential value of +0.3 V using DPV study. The HQ current density is increased linearly from 0.1 to 100 μM concentration and its corresponding plot is shown in Fig. 12b with correlation coefficient (R^2) value of 0.9961.

3.6. Amperometric (i-t curve)

The amperometric i-t curve is obtained for determination of HQ using $FeWO_4/SnO_2$/Nf modified GCE in 0.1 M PBS (pH = 7.0) at an applied potential of +0.21 V as shown in Fig. 13a. The $FeWO_4/SnO_2$/Nf immobilized GCE electrode shows an initial current response for 0.01 μM HQ. Further, the successive injections of 0.01 μM HQ in each step with a 50 s time interval, the peak current increases and steady-state current response is attained within 3 s, which demonstrates

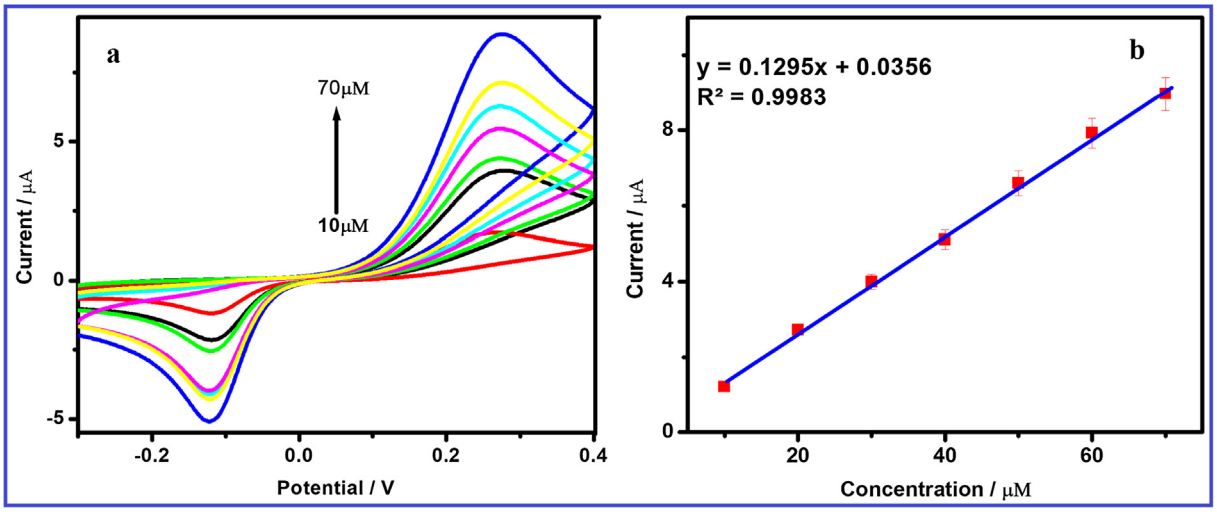

Fig. 9 (a) Cyclic voltammetric response of $FeWO_4/SnO_2$/Nf immobilized modified GC electrode varying 10 μM HQ concentration in the range from 10 to 70 μM in 0.1 M PBS (pH = 7) and 7 (b) Inset: calibration plot in concentration vs current.

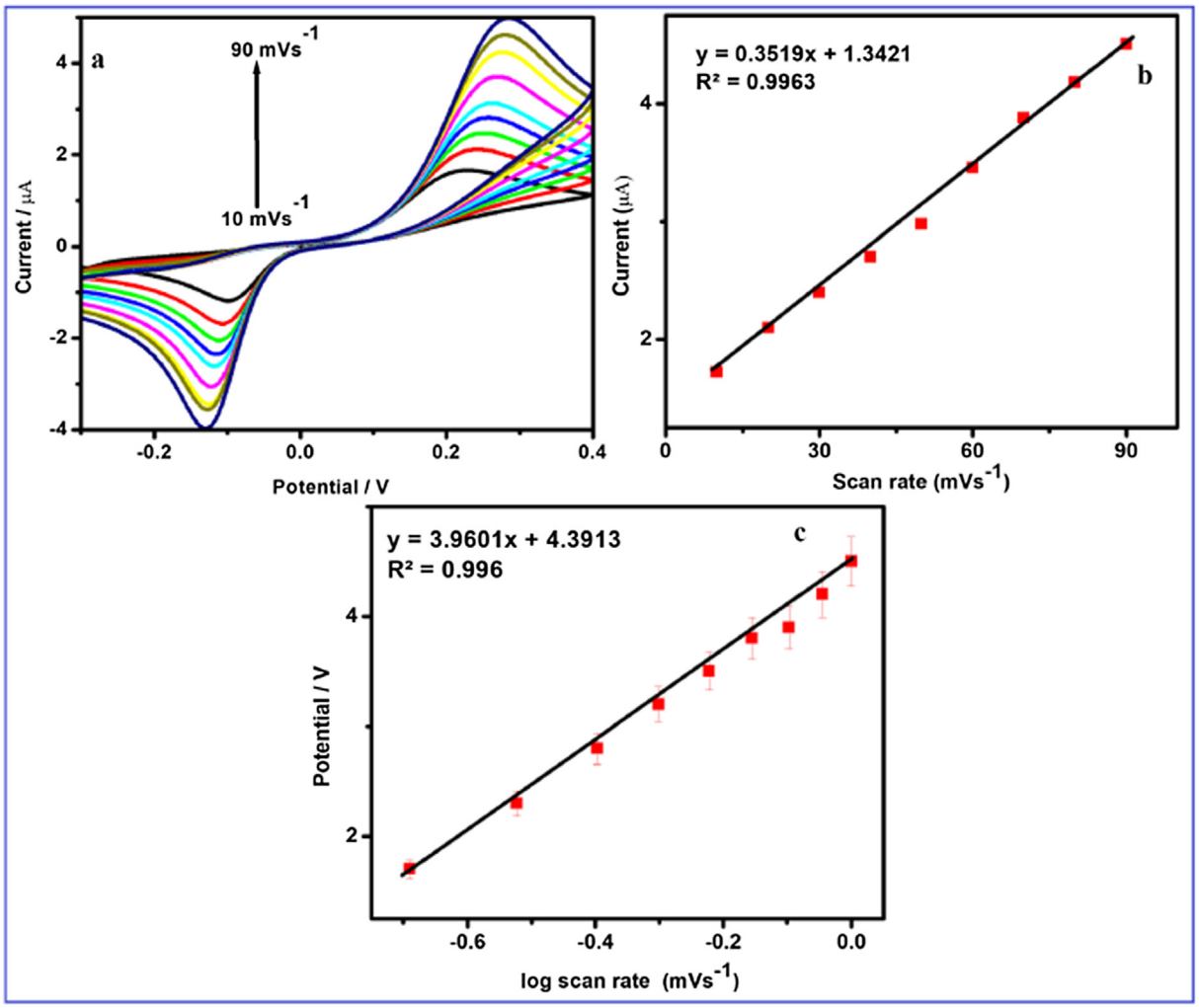

Fig. 10 Cyclic voltammetric responses of $FeWO_4/SnO_2$/Nf immobilized modified GC electrode in 0.1 M PBS (pH 7.0) at scan rates: (a) 10, 20, 30, 40, 50, 60, 70, 80, and 90 mV s^{-1}, (b) Plots of peak currents vs. scan rate and (c) Plots of peak potential vs. log of scan rate.

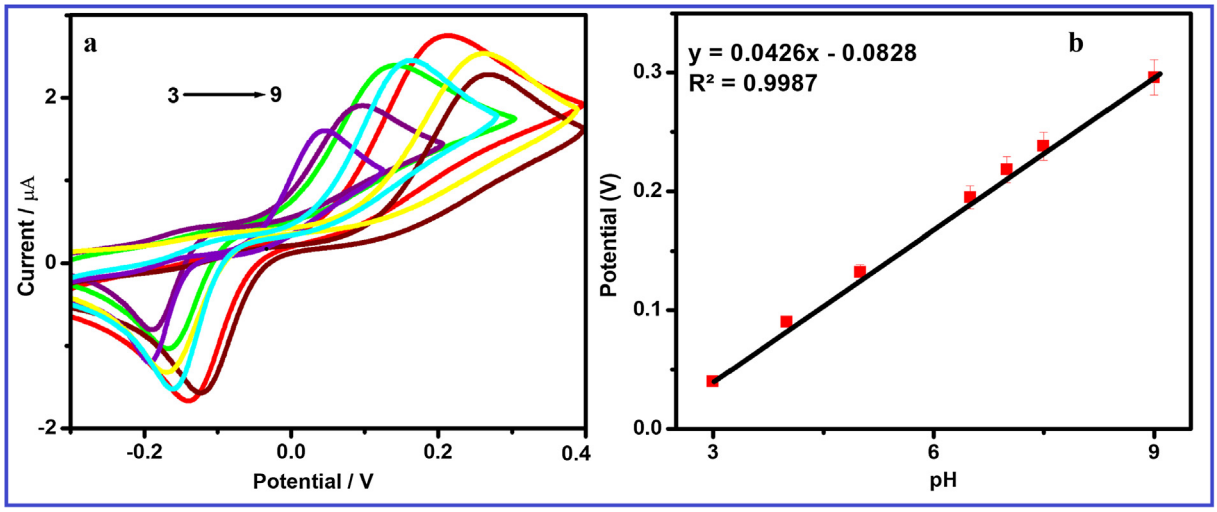

Fig. 11 (A) Cyclic voltammograms obtained at $FeWO_4/SnO_2$/Nf immobilized modified GC electrode in 10 µM HQ containing different pH (pH 3, 4.5, 5.5, 6.5, 7, 8 and 9) at a scan rate of 100 mV/s and (B) Calibration plot for the pH vs peak potential for the detection of HQ.

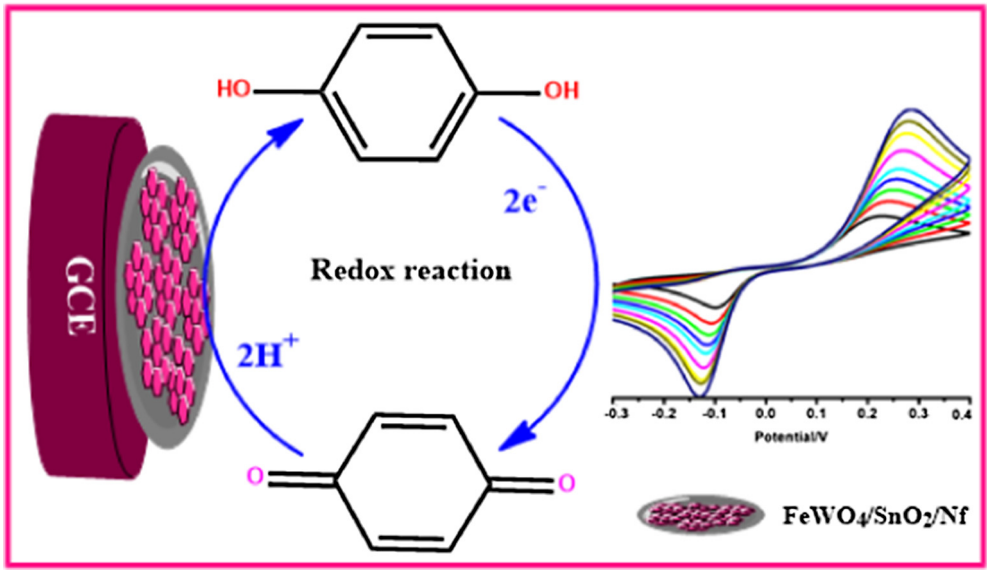

Scheme 2 The plausible electrocatalytic mechanism of HQ on of $FeWO_4/SnO_2$/Nf immobilized modified GC electrode.

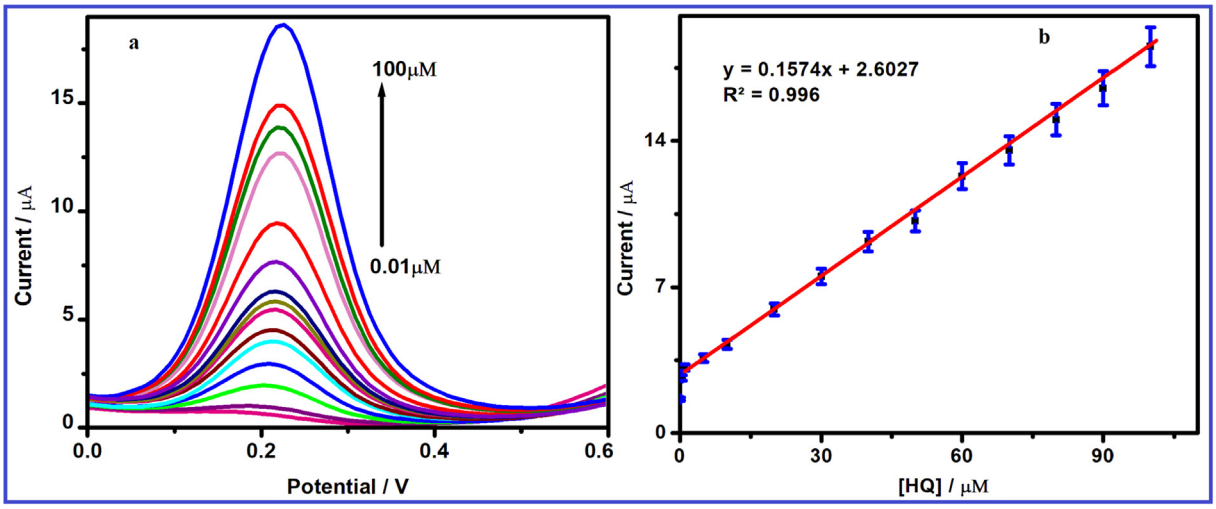

Fig. 12 DPV response of $FeWO_4/SnO_2$/Nf immobilized modified GC electrode in the absence (bottom curve) and presence of different concentration (0.1–100 μM) of 10 μM HQ containing pH 7.0. (b) Linear plot for (HQ) vs. current response.

that the fast amperometric response to the oxidation of HQ (Palanisamy et al., 2014; Ding et al., 2005 Yu et al., 2009; Awua et al., 2018). The linear relationship between the peak current with respect to concentration of HQ, ranging from 0.01 μM to 50 μM at $FeWO_4/SnO_2$/Nf immobilized GCE with correlation coefficient of R^2 is 0.9860 is shown in Fig. 13b. The low detection limit (LOD) is calculated using the following equations for the determination of HQ using the present electrochemical sensor.

$$LOD = 3.3s/b$$

$$LOD = 10s/b$$

where 'S' standard deviation of HQ, 'b' slope of calibration curve. The detection limit is found to be 0.0013 μM (S/N = 3) and sensitivity 12.06 μA μM^{-1} cm^{-2} respectively. The obtained data show that the $FeWO_4/SnO_2$/Nf immobilized GCE has an excellent sensitivity, low detection limit and better linear relationship as presented in Table 2 (Chen et al., 2017a, 2017b, 2011, 2019; Karim-Nezhad et al., 2017; Zheng et al., 2013; Palanisamy et al., 2014; Li et al., 2012; Wang et al., 2013; Yuan et al., 2013; Zan et al., 2016; Gan et al., 2013; Yang et al., 2019; Guo et al., 2012; Fan et al., 2019; Ahmed et al., 2018).

3.7. Reproducibility, stability and selectivity

Under the optimized experimental conditions, the reproducibility of the fabricated electrochemical sensor is investigated in 0.1 μM of HQ concentration by comparing the peak currents in the solution phase. Additionally five different electrodes are used for the successive investigation of reproducibil-

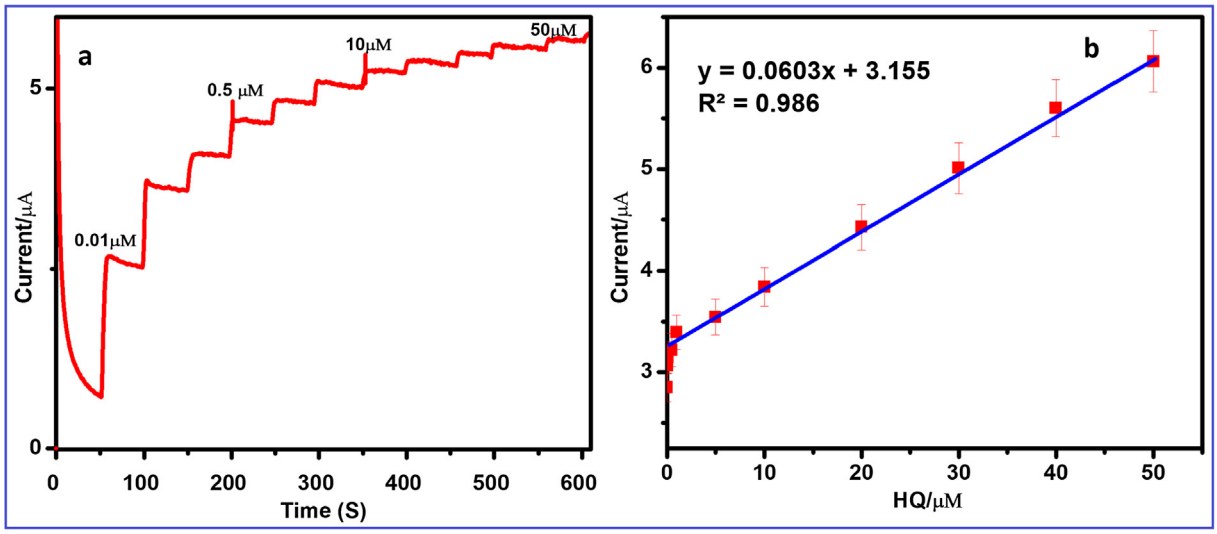

Fig. 13 (a) Amperometric i–t curve for the determination of HQ at $FeWO_4/SnO_2$/Nf immobilized modified GC electrode in 0.1 M PBS (pH 7.0). Each addition increases the concentration of 0.01 μM of HQ at a regular interval of 50 s, (b) the calibration plot for the linear dependence of peak current vs concentrations of HQ.

Table 2 Analytical comparison of $FeWO_4/SnO_2$/Nf immobilized modified GCE with previously reported modified electrodes for determination of HQ.

Modified electrode	Method	pH	LOD (μM)	Linear response range (μM)	Ref
ND/GCE	DPV	7.0	0.19	1.0–78.0	Chen et al. (2017a, 2017b)
AuNPs/Cy-acid/GCE	DPV	7.0	0.02	2.99–39.2	Karim-Nezhad et al. (2017)
RGO/PDA/GCE	DPV	4.5	0.74	1.0–230.0	Zheng et al. (2013)
RGO/Cu-NPs/GCE	LSV	7.0	0.032	3.0–350.0	Palanisamy et al. (2014)
TRGO/GCE	DPV	6.0	0.75	1.0–500.0	Li et al. (2012)
AuNPs/SGR/GCE	DPV	5.6	1.0	5.0–100.0	Wang et al. (2013)
GMC/GCE	DPV	3.0	0.37	2.0–50.0	Yuan et al. (2013)
ERGO/GCE	DPV	5.8	0.2	6.0–200.0	Chen et al. (2011)
N-RGO/GCE	DPV	7.0	0.1	5–693	Zan et al. (2016)
GO–MnO_2/GCE	DPV	7.0	0.07	0.01–0.7	Gan et al. (2013)
MWCNT/RGO	DPV	7.0	3.89	15–921	Yang et al. (2019)
Carbon nanofibers/GCE	DPV	4.7	0.4	1–200	Guo et al. (2012)
GCE	DPV	6.7	0.06	0.5–3.0	Fan et al. (2019)
SrO, NiO, ZnO /GCE	DPV	7.0	2.3 ± 0.1 pm	0.40 nM-0.02 M	Ahmed et al. (2018)
Au3@Pd6/GCE	DPV	7.0	0.63	4–5000	Chen et al. (2019)
Pt/poly –CD/MWCNT	DPV	6.0	0.015	0.05–565	Huang et al. (2018)
$FeWO_4/SnO_2$/Nf/GCE	Amperometric	7.0	0.0013	0.01–100	This work

ity of the proposed HQ sensor. The obtained electrochemical data for the five different electrodes show that the relative standard deviation (RSD) of 3.4%,which infers that the present modified electrode shows good reproducibility after the successful repeated experiments (Dong et al., 2008; Wang et al., 2018; Lin et al., 2018). The 30 repeated CVs were taken to study the repeatability of $FeWO_4/SnO_2$/Nf immobilized GCE surface using 10 μM HQ and found to be a relative standard deviation of 2.84%. This is also indicated that the present modified electrochemical sensor possessed good repeatability as shown in Fig. 14a. After 30 days the peak current of 10 μM HQ is decreased by less than 3 ± 0.02%. Moreover, the stability of $FeWO_4/SnO_2$/Nf immobilized modified GCE is also tested and it is kept in desiccators at room temperature for 30 days. After 30 days, the obtained CV for the determination of HQ using the $FeWO_4/SnO_2$/Nf immobilized modified GCE shows a very minimum decrement of peak current values, which indicates that the present electrochemical sensor shows good stability. The selectivity of the biological interferents is used for determination of HQ at $FeWO_4/SnO_2$/Nf immobilized GCE surface. The biological interferents such as (a) hydroquinone (HQ), (b) resorcinol (RC) and (c) catechol (CC), neurotransmitters (d) serotonin (SR), (e) dopamine (DA), (f) uric acid (UA), (g) ascorbic acid (AA), (h) cysteine (Cys), (i) norepinephrine (NEP) and (j) glucose (GLU) in 0.1 M PBS (pH = 7.0) are used for determination of HQ at $FeWO_4/SnO_2$/Nf immobilized GCE by amperometric technique. The obtained amperometric current response is shown in Fig. 14b. Fig. 14b clearly shows that the 100 fold excess of RC, CC, SR, DA, UA, AA, Cys, NEP and GLU doesn't

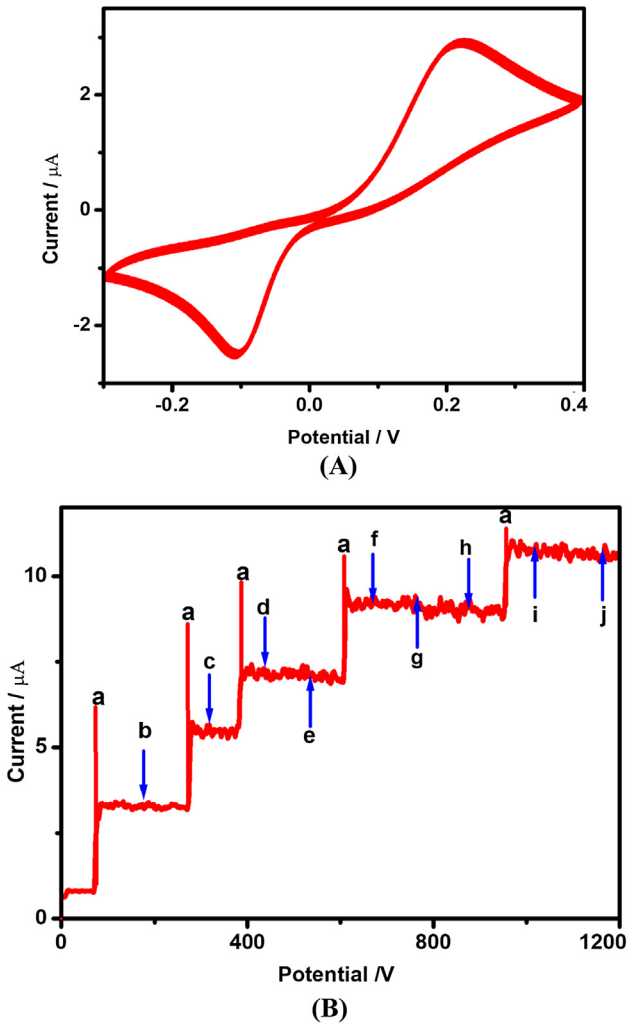

Fig. 14 (A) Cyclic voltammetric response of $FeWO_4/SnO_2$/Nf immobilized modified GC electrode (30 cycles) confirming the stability of the sensor system in 10 μM nicotine containing 0.1 M (pH = 7) PBS. (B) Amperometric response for $FeWO_4/SnO_2$/Nf immobilized modified GC electrode to successive addition of 10 μM nicotine (a) in the presence of 100-fold excess of concentrations of (b) AA, (c) DA, (d) UA, (e) EP, (f) NEP, (g) CY, (h) HQ and (i) GLU with homogenous stirring in 0.1 M PBS (pH = 7) at a potential of +0.2 V.

influence the steady-state current response. Thus, $FeWO_4/SnO_2$/Nf immobilized GCE exhibits a better selectivity and high sensitivity towards the detection of HQ. The overall result indicates that the present electrochemical sensor may be used for selective determination of HQ among the various interferents (Zou et al., 2017; Chen et al., 2017a, 2017b).

3.8. Analysis of real samples

In order to evaluate the determination of HQ, the present electrochemical sensor has been applied to environmental real samples such as tap water, lake water and river water samples to a known amount of HQ is added. The water samples were collected from Vaigai river side, Madurai. The collected water samples are used without pretreatment and 0.1 M PBS was used to maintained pH of the medium. The standard addition method is used for the accurate determination of HQ in this present study. The obtained data are given in Table 3. Table 3 clearly indicates that the recovery results are varied from 96.9% to 105.7%. This result reveals that the present modified electrode has a potential application for the detection of HQ in real samples. Additionally, the RSD values ranging from 2.8% to 3.9%, which confirms that the accuracy of this technique and also reveals that the proposed electrochemical sensor has acceptable reliability for determination HQ in different water samples.

Table 3 Experimental results for detection of HQ in different water samples.

Sample	Added (μM)	Founded (μM)	RSD (%)	Recovery (%)
Tap water	5.0	4.89	3.4	98.5
	10.0	10.28	3.2	102.8
Lake water	5.0	5.29	3.9	105.7
	10.0	10.30	2.9	103.0
River water	5.0	4.89	3.7	96.9
	10.0	10.26	2.8	102.6

4. Conclusion

In summary, $FeWO_4/SnO_2$ nanocomposite is synthesized using the sonication method and applied to fabricate a novel electrochemical sensor for the successful detection of HQ. The $FeWO_4/SnO_2$/Nf immobilized GCE shows better electrochemical sensing ability towards HQ detection, which is observed by increasing of peak current. Moreover, the $FeWO_4/SnO_2$/Nf immobilized GCE provides excellent stability, sensitivity, reproducibility and anti-interference ability. The $FeWO_4/SnO_2$/Nf immobilized GCE is successfully applied to detect HQ in different water samples and also the satisfied results are obtained. The proposed nanocomposite modified electrochemical sensing method is simple and has a potential impact on HQ detection in real samples.

Acknowledgement

The authors thank the UGC Networking Resource Centre, School of Chemistry, University of Hyderabad, Telangana, India, for providing necessary laboratory facilities to carry out this work. The authors thank the Management of Thiagarajar College for providing necessary laboratory facilities to carry out this work.

References

Ahammad, A.J.S., Rahman, M.M., Xu, G.R., Kim, S., Lee, J.J., 2011. Highly sensitive and simultaneous determination of hydroquinone and catechol at poly(thionine) modified glassy carbon electrode. Electrochim. Acta. 56, 5266–5271.

Ahmed, J., Rahman, M.M., Siddiquey, I.A., Asiri, A.M., Hasnat, M. A., 2018. Efficient hydroquinone sensor based on zinc, strontium and nickel based ternary metal oxide (TMO) composites by differential pulse voltammetry. Sens. Actuat. B 256, 383–392.

Alam, M.K., Rahman, M.M., Abbas, M., Torati, S.R., Asiri, A.M., Kim, D., GiKim, C., 2017. Ultra-sensitive 2-nitrophenol detection based on reduced graphene oxide/ZnO nanocomposites. J. Electroanal. Chem. 788, 66–73.

Almeida, M.G., Silveira, C.M., Moura, J.J.G., 2007. Biosensing nitrite using the system nitrite redutase/Nafion/methyl viologen—a voltammetric study. Biosens. Bioelectron. 22, 2485–2492.

Amano, F., Nogami, K., Abe, R., Ohtani, B., 2008. Preparation and characterization of bismuth tungstate polycrystalline flake-ball particles for photocatalytic reactions. J. Phy. Chem. C 112, 9320–9326.

Arshad, M.N., AliSheikh, T., Rahman, M.M., Asiri, A.M., Marwani, H.M., Awual, Md.R., 2017. Fabrication of cadmium ionic sensor based on (E)-4-Methyl-N′-(1-(pyridin-2-yl) ethylidene)benzenesulfonohydrazide (MPEBSH) by electrochemical approach. J. Organomet. Chem. 827, 49–55.

Aslam, A., Khan, P., Khan, A., Rahman, M.M., Asiri, A.M., Oves, M., 2017. Sensor development of 1, 2 Dichlorobenzene based on polypyrole/Cu-doped ZnO (PPY/CZO) nanocomposite embedded silver electrode and their antimicrobial studies. Int. J. Biol. Macromol 98, 256–267.

Awua, Md.R., Khraisheh, M., Alharthi, N.H., Luqman, M., Islam, A., Karim, M.R., Rahman, M.M., Khaleque, Md.A., 2018. Efficient detection and adsorption of cadmium(II) ions using innovative nano-composite materials. Chem. Eng. J. 343, 118–127.

Awual, Md.R., Hasan, Md.M., Eldesoky, G.E., Khaleque, Md.A., Rahman, M.M., Naushad, Mu., 2016. Facile mercury detection and removal from aqueous media involving ligand impregnated conjugate nanomaterials. Chem. Eng. J. 290, 243–251.

Awual, Md.R., Alharthi, N.H., Hasan, Md.M., Karim, M.R., Islam, A., Znad, H., Hossain, M.A., Halim, Md.E., Rahman, M.M., Khaleque, Md.A., 2017a. Inorganic-organic based novel nano-conjugate material for effective cobalt(II) ions capturing from wastewater. Chem. Eng. J. 324, 130–139.

Awual, Md.R., Alharthi, N.H., Okamoto, Y., Karim, M.R., Halim, Md.E., Hasan, Md.M., Rahman, M.M., Islam, Md.M., Khaleque, Md.A., Sheikh, Md.C., 2017b. Ligand field effect for Dysprosium(III) and Lutetium(III) adsorption and EXAFS coordination with novel composite nanomaterials. Chem. Eng. J. 320, 427–435.

Azad, U.P., Ganesan, V., 2010a. Influence of metal nanoparticles on the electrocatalytic oxidation of glucose by Poly(Ni^{II}teta) modified electrodes. Electroanalysis 22, 575–583.

Azad, U.P., Ganesan, V., 2010b. Efficient sensing of nitrite by Fe$(bpy)_3^{2+}$ immobilized Nafion modified electrodes. Chem. Commun. 46, 6156–6158.

Bhosale, R., Jain, S., Vinod, C.P., Kumar, S., Ogale, S., 2019. Direct Z-scheme g-C_3N_4/$FeWO_4$ nanocomposite for enhanced and selective photocatalytic CO_2 reduction under visible light. ACS Appl. Mater. Interfaces 11, 6174–6183.

Chen, T.W., Palanisamy, S., Chen, S.M., Velusamy, V., Liu, Y.H., Tseng, T.W., Yu, M.C., Lee, S.Y., Chang, W.H., Liu, X., 2017a. Sensitive and low-potential electrochemical detection of hydroquinone using a nanodiamond modified glassy carbon electrode. Int. J. Electrochem. Sci. 12, 8021–8032.

Chen, T.W., Palanisamy, S., Chen, S.M., Velusamy, V., Ramaraj, S. K., 2017b. A novel Amperometric Gallic acid Sensor based on Polymelamine entrapped Graphene Composite. Int. J. Electrochem. Sci. 12, 4107–4119.

Chen, L., Tang, Y., Wang, K., Liu, C., Luo, S., 2011. Direct electrodeposition of reduced graphene oxide on glassy carbon electrode and its electrochemical application. Electrochem. Commun. 13, 133–137.

Chen, T., Xa, J., Arsalan, M., Sheng, Q., Zheng, J., Cao, W., Yue, T., 2019. Controlled synthesis of Au@Pd core-shell nanocomposites and their application for electrochemical sensing of hydroquinone. Talanta 198, 78–85.

Ciucu, A.A., 2014. Chemically modified electrodes in biosensing. J. Biosens. Bioelectron. 5, 2–10.

Cui, H., Zhang, Q.L., Myint, A., Ge, X.W., Liu, L.J., 2006. Chemiluminescence of cerium (IV)-rhodamine 6G-phenolic compound system. J. Photochem. Photobiol. A 181, 238–245.

Dadigala, R., Bandi, R., Reddy Gangapuram, B., Guttena, V., 2019. Construction of in situ self-assembled $FeWO_4$/g-C_3N_4 nanosheet heterostructured Z-schemephotocatalysts for enhanced photocatalyticdegradation of rhodamine B and tetracycline. Nanoscale Adv. 1, 322–333.

Dai, X.J., Luo, Y.S., Zhang, W.D., Fu, S.Y., 2010. Facile hydrothermal synthesis and photocatalytic activity of bismuth tungstate hierarchical hollow spheres with an ultrahigh surface area. Dalton Trans. 39, 3426–3432.

Ding, Y.P., Liu, W.L., Wu, Q.S., Wang, X.G., 2005. Direct simultaneous determination of dihydroxybenzene isomers at C-nanotube-modified electrodes by derivative voltammetry. J. Electroanal Chem. 575, 275–280.

Dong, J., Qu, X., Wang, L., Zhao, C., Xua, J., 2008. Electrochemistry of Nitrogen-Doped Carbon Nanotubes (CNx) with different nitrogen content and its application in simultaneous determination of dihydroxybenzene isomers. Electroanalysis 20, 1981–1986.

Fan, J., Pang, J., Zhang, Y., Zhang, L., Xu, W., Wang, J., 2019. Simultaneous detection of hydroquinone and catechol with decreasing pH at a bare glassy carbon electrode surface. Anal. Methods 11, 604–609.

Fukai, Y., Kondo, Y., Mori, S., Suzuki, E., 2007. Highly efficient dye-sensitized SnO_2 solar cells having sufficient electron diffusion length. Electrochem. Commun. 9, 1439–1443.

Gan, T., Sun, J., Huang, K., Song, L., Li, Y., 2013. A graphene oxide–mesoporous MnO_2 nanocomposite modified glassy carbon electrode as a novel and efficient voltammetric sensor for simultaneous determination of hydroquinone and catechol. Sens. Actuat. B 177, 412–418.

Ganesan, V., John, S.A., Ramaraj, R., 2001. Multielectrochromic properties of methylene blue and phenosafranine dyes incorporated into Nafion film. J. Electroanal. Chem. 502, 167–173.

Ganesan, V., Ramaraj, R., 2001. Electrocatalytic oxidation of hydrogen peroxide by poly (NiIIteta) modified electrodes. J. Appl. Electrochem. 31, 585–590.

Garcia-Mesa, J.A., Mateos, R., 2007. Direct automatic determination of bitterness and total phenolic compounds in virgin olive oil using a pH-based flow-injection analysis system. J. Agric. Food Chem. 55, 3863–3868.

Guo, Q., Huang, J., Chen, P., Liu, Y., Hou, H., You, T., 2012. Simultaneous determination of catechol and hydroquinone using electrospun carbon nanofibers modified electrode. Sens. Actuators B 163, 179–185.

Guo, X., Yang, J., Deng, Y., Wei, H., Zhao, D., 2010. Hydrothermal synthesis and photoluminescence of hierarchical lead tungstate superstructures: effects of reaction temperature and surfactants. Eur. J. Inorg. Chem. 11, 1736–1742.

Hu, S., Wang, Y., Wang, X., Xu, L., Xiang, J., Sun, W., 2012. Electrochemical detection of hydroquinone with a gold nanoparticle and graphene modified carbon ionic liquid electrode. Sens. Actuat. B Chem. 168, 27–33.

Hu, W., Zhao, Y., Liu, Z., Dunnill, C.W., Gregory, D.H., Zhu, Y., 2008. Nanostructural evolution: from one-dimensional tungsten oxide nanowires to three-dimensional ferberite flowers. Chem. Mater. 20, 5657–5665.

Huan, S.Y., Chu, H., Jiao, C.X., Zeng, G.M., Huang, G.H., Shen, G. L., Yu, R.Q., 2004. Selective electrochemical molecular recognition of benzenediol isomers using molecularly imprinted TiO_2 film electrodes. Anal. Chim. Acta 506, 31–39.

Huang, X., Deng, X., Qi, W., Wu, D., 2018. Simultaneous detection of hydroquinone and catechol using platinum nanoparticles decorated graphene/poly-cyclodextrin/multiwalled carbon nanotubes (MWCNTs) nanocomposite based biosensor. J. Nanosci. Nanotechnol. 18, 8118–8123.

Hussain, M.M., Rahman, M.M., Asiri, A.M., 2017a. Ultrasensitive and selective 4-aminophenol chemical sensor development based on nickel oxide nanoparticles decorated carbon nanotube nanocomposites for green environment. J. Environ. Sci. 53, 27–38.

Hussain, M.M., Rahman, M.M., Arshad, M.N., Asiri, A.M., 2017b. Hg^{2+} Sensor development based on (E)-N′-nitrobenzylidene-benzene sulfonohydrazide (NBBSH) derivatives fabricated on a glassy carbon electrode with a Nafion matrix. ACS Omega 2, 420–443.

Ingo, P., Viktor, H., Sören, K., Vasilii, C., Oleg, L., Tudor, B., Viola, D., Ion, T., Lorenz, K., Rainer, A., Yogendra Kumar, M., 2015. Three-dimensional SnO_2 nanowire networks for multifunctional applications: from high-temperature stretchable ceramics to ultra-responsive sensors. Adv. Electron. Mater. 1500081, 1–8.

Jenita Rani, G., Sathiya, S.M., Jothi Rajan, M.A., 2016. Self-assembled rGO/$FeWO_4$ flower structures by a solvothermal reaction with enhanced catalytic activity for dye degradation. Chem. Sci. Rev. Lett. 5, 101–109.

Jiang, J., Du, X., 2014. Sensitive electrochemical sensors for simultaneous determination of ascorbic acid, dopamine, and uric acid based on Au@Pd-reduced graphene oxide nanocomposites. Nanoscale 6, 11303–11309.

Jiang, L., Gu, S., Ding, Y., Jiang, F., Zhang, Z., 2014. Facile and novel electrochemical preparation of a graphene-transition metal oxide nanocomposite for ultrasensitive electrochemical sensing of acetaminophen and phenacetin. Nanoscale 6, 207–214.

Karim-Nezhad, G., Moghaddam, M.H., Khorablou, Z., Dorraji, P.S., 2017. L- cysteine based polymer matrix decorated with Au-nanoparticles: as a sensing platform for simultaneous determination of hydroquinone and catechol. J. Electrochem. Soc. 164, 193–199.

Karthika, A., Ramasamy Raja, V., Karuppasamy, P., Suganthi, A., Rajarajan, M., 2019. Electrochemical behaviour and voltammetric determination of mercury (II) ion in cupricoxide/polyvinylalcohol nanocomposite modified glassy carbon electrode. Microchem. J. 145, 737–744.

Kloprogge, J.T., Weier, M.L., Duong, L.V., Frost, R.L., 2004. Microwave-assisted synthesis and characterisation of divalent metal tungstate nanocrystalline minerals: ferberite, hübnerite, sanmartinite, scheelite and stolzite. Mater. Chem. Phys. 88, 438–443.

Kova'cs, A., Mo'rtl, M., Kende, A., 2011. Development and optimization of a method for the analysis of phenols and chlorophenols from aqueous samples by gas chromatography–mass spectrometry, after solid-phase extraction and trimethylsilylation. Microchem. J. 99, 125–131.

Lang, X., Hirata, A., Fujita, T., Chen, M., 2011. Nanoporous metal/oxide hybrid electrodes for electrochemical supercapacitors. Nat. Nanotech. 6, 232–236.

Laviron, E., 1979. General expression of the linear potential sweep voltammogram in the case of diffusionless electrochemical systems. J. Electroanal. Chem. 101, 19–28.

Li, J., Liu, C.Y., Cheng, C., 2011. Electrochemical detection of hydroquinone by graphene and Pt–graphene hybrid material synthesized through a microwave-assisted chemical reduction process. Electrochim. Acta 56, 2712–2716.

Li, S.J., Qian, C., Wang, K., Hua, B.Y., Wang, F.B., Sheng, Z.H., Xia, X.H., 2012. Application of thermally reduced graphene oxide modified electrode in simultaneous determination of dihydroxybenzene isomers. Sens. Actuat. B 174, 441–448.

Lin, Q., Jiang, X.M., Ma, X.Q., Liu, J., Yao, H., Zhang, Y.M., Wei, T. B., 2018. Novel bispillar [5] arene-based AIEgen and its' application in mercury(II) detection. Sensors Actuat. B: Chem. 272, 139–145.

Liu, C., Li, W., Gu, Y., Hao, S., Yan, X., Zhang, Z., Yang, M., 2014. Simultaneous determination of catechol and hydroquinone based on poly (sulfosalicylic acid)/functionalized graphene modified electrode. J. Appl. Electrochem. 44, 1059–1067.

Marrubini, G., Calleri, E., Coccini, T., Castoldi, A.F., Manzo, L., 2005. Direct analysis of phenol, catechol and hydroquinone in human urine by coupled-column HPLC with fluorimetric detection. Chromatographia 62, 25–31.

Mattioli, G., Melis, C., Malloci, G., Filippone, F., Alippi, P., Giannozzi, P., Mattoni, A., Bonapasta, A.A., 2012. Zinc oxide-zinc phthalocyanine interface for hybrid solar cells. J. Phy. Chem. C 116, 15439–15448.

Mishra, B., Kumbhare, L., Jain, V., Priyadarsini, K., 2008. Pulse radiolysis studies on reactions of hydroxyl radicals with selenocystine derivatives. J. Phys. Chem. 112, 4441–4446.

Palanisamy, S., Karuppiah, C., Chen, S.M., Yang, C.Y., Periakaruppan, P., 2014. Simultaneous and selective electrochemical determination of dihydroxybenzene isomers at a reduced graphene oxide and copper nanoparticles composite modified glassy carbon electrode. Anal. Methods 6, 4271–4278.

Perfecto, T.M., Zito, C.A., Volanti, D.P., 2016. Room-temperature volatile organic compounds sensing based on $WO_3.0.33H_2O$, hexagonal-WO_3, and their reduced graphene oxide composites. RSC Adv. 6, 105171–105179.

Pistonsei, M., Zezio, M.D., Centurio'n, M., Palomeque, M., Lista, A., Ferna'ndez, B., 2006. Determination of phenol, resorcinol and hydroquinone in air samples by synchronous fluorescence using partial least-squares (PLS). Talanta 69, 1265–1268.

Rahman, M.M., 2018. Label-free Kanamycin sensor development based on CuO-NiO hollow-spheres: food samples analyses. Sens. Actuat. B Chem. 264, 84–91.

Rahman, M.M., Asiria, A.M., 2015. Fabrication of highly sensitive ethanol sensor based on doped nanostructure materials using tiny chips. RSC Adv. 5, 63252–63263.

Rahman, M.M., Ahmed, J., Asiri, A.M., 2017a. A glassy carbon electrode modified with γ-Ce_2S_3-decorated CNT nanocomposites for uric acid sensor development: a real sample analysis. RSC Adv. 7, 14649–14659.

Rahman, M.M., Alfonso, V.G., Santiago, F.F., Bisquert, J., Asiri, A. M., Alshehri, A.A., Albar, H.A., 2017b. Hydrazine sensors development based on a glassy carbon electrode modified with a nanostructured TiO_2 films by electrochemical approach. Microchim. Acta 184, 2123–2129.

Rahman, M.M., Alam, M.M., Asiri, A.M., Islam, M.A., 2017c. Ethanol sensor development based on ternary-doped metal oxides (CdO/ZnO/Yb_2O_3) nanosheets for environmental safety. RSC Adv. 7, 22627–22639.

Rahman, M.M., Alam, M.M., Asiri, A.M., Islam, M.A., 2017d. Fabrication of selective chemical sensor with ternary ZnO/SnO_2/Yb_2O_3 nanoparticles. Talanta 170, 215–223.

Ribeiro, G.H., Vilarinho, L.M., Ramos, T.S., Bogado, A.L., Dinelli, L.R., 2015. Electrochemical behaviour of hydroquinone and catechol at glassy carbon electrode modified by electro polymerization of tetra ruthenated oxo vanadium porphyrin. Electrochim. Acta 176, 394–401.

Saravanakumar, K., Muthuraj, K., 2017. Fabrication of sphere like plasmonic Ag/SnO_2 photocatalyst for the degradation of phenol. Optik – Int. J. Light Electron. Opt. 131, 754–763.

Selvarajan, S., Suganthi, A., Rajarajan, M., 2018a. A simple sonochemical approach to fabricate a urea biosensor based on zinc phthalocyanine/graphene oxide/urease bioelectrode. Ultrason. Sonochem. 42, 183–192.

Selvarajan, S., Suganthi, A., Rajarajan, M., 2018b. Fabrication of g-C_3N_4/NiO heterostructured nanocomposite modified glassy carbon electrode for quercetin biosensor. Ultrason. Sonochem. 41, 651–660.

Solis, J.L., Saukko, S., Kish, L., Granqvist, C.G., Lantto, V., 2001. Semiconductor gas sensors based on nanostructured tungsten oxide. Thin Solid Films 391, 255–260.

Turdean, G.L., Popescu, I.C., Curulli, A., Palleschi, G., 2006. Iron (III) protoporphyrin IX—single-wall carbon nanotubes modified electrodes for hydrogen peroxide and nitrite detection. Electrochim. Acta 51, 6435–6441.

Umar, A., Rahman, M.M., Kim, S.H., Hahn, Y.B., 2008. Zinc oxide nanonail based chemical sensor for hydrazine detection. Chem. Commun. 2, 166–168.

Vignesh, K., Priyanka, R., Hariharan, R., Rajarajan, M., Suganthi, A., 2014. Fabrication of CdS and $CuWO_4$ modified TiO_2 nanoparticles and its photocatalytic activity under visible light irradiation. J. Ind. Eng. Chem. 20, 435–443.

Wang, L., Meng, Y., Chen, Q., Deng, J., Zhang, Y., Li, H., Yao, S., 2013. Simultaneous electrochemical determination of dihydroxybenzene isomers based on the hydrophilic carbon nanoparticles and ferrocene-derivative mediator dual sensitized graphene composite. Electrochim. Acta 92, 216–225.

Wang, J., Zhang, K., Xu, H., Yan, B., Gao, F., Shi, Y., Du, Y., 2018. Engineered photo electrochemical platform for the ultrasensitive detection of caffeic acid based on flower-like MoS_2 and PANI nanotubes nanohybrid. Sensors Actuat. B: Chem. 276, 322–330.

Wu, Z.S., Zhou, G., Yin, L.C., Ren, W., Li, F., Cheng, H.M., 2012. Graphene/metal oxide composite electrode materials for energy storage. Nano Energy 1, 107–131.

Xie, T., Liu, Q., Shi, Y., Liu, Q., 2006. Simultaneous determination of positional isomers of benzenediols by capillary zone electrophoresis with square wave amperometric detection. J. Chromatogr. A. 1109, 317–321.

Yang, S., Yang, M., Liu, Q., Wang, X., Fa, H., Wang, Y., Hou, C., 2019. An ultrasensitive electrochemical sensor based on multiwalled carbon nanotube@reduced graphene oxide nanoribbon composite for simultaneous determination of hydroquinone, catechol and resorcinol. J. Electrochem. Soc. 166, 547–553.

Yao, Y., Liu, Y., Yang, Z., 2016. A novel electrochemical sensor based on glassy carbon electrode modified with Cu-MWCNTs nanocomposite for determination of hydroquinone. Anal. Methods 8, 2568–2575.

Yu, J., Du, W., Zhao, F., Zeng, B., 2009. High sensitive simultaneous determination of catechol and hydroquinone at mesoporous carbon CMK-3 electrode in comparison with multi-walled carbon nanotubes and Vulcan XC-72 carbon electrodes. Electrochim. Acta. 54, 984–988.

Yu, S.H., Liu, B., Mo, M.S., Huang, J.H., Liu, X.M., Qian, Y.T., 2003. General synthesis of single-crystal tungstate nanorods/nanowires: a facile, low-temperature solution approach. Adv. Funct. Mater. 13, 639–647.

Yuan, X., Yuan, D., Zeng, F., Zou, W., Tzorbatzoglou, F., Tsiakaras, P., Wang, Y., 2013. Preparation of graphitic mesoporous carbon for the simultaneous detection of hydroquinone and catechol. Appl. Catal. B 129, 367–374.

Zan, Lu., Dongning, Li, Zhang, Q., Wei, J., 2016. Facile simultaneous determination of hydroquinone and catechol using nitrogen-doped graphene modified electrode. Int. J. Electrochem. Sci. 11, 10607–10619.

Zhang, L., Sh, J., Huang, Y., Xu, H., Xu, K., Chu, P.K., Ma, F., 2019. Octahedral SnO_2/graphene composites with enhanced gas-sensing performance at room temperature. ACS Appl. Mater. Interfaces 11, 2958–12967.

Zhang, Q., Yao, W.T., Chen, X., Zhu, L., Fu, Y., Zhang, G., Shengs, L., Yu, S.H., 2007. Nearly monodisperse tungstate MWO_4 microspheres (M = Pb, Ca): surfactant-assisted solution synthesis and optical properties. Cryst. Growth Des. 7, 1423–1431.

Zheng, L., Xiong, L., Li, Y., Xu, J., Kang, X., Zou, Z., Yang, S., Xia, J., 2013. Facile preparation of polydopamine-reduced graphene oxide nanocomposite and its electrochemical application in simultaneous determination of hydroquinone and catechol. Sens. Actuat. B 177, 344–349.

Zhou, J., Li, X., Yang, L.L., Yan, S.L., Wang, M.M., Cheng, D., Chen, Q., Dong, Y.L., Liu, P., Cai, W.Q., Zhang, C.C., 2015. The Cu-MOF-199/single-walled carbon nanotubes modified electrode for simultaneous determination of hydroquinone and catechol with extended linear ranges and lower detection limits. Anal. Chim. Acta. 899, 57–65.

Zhou, Y.X., Yao, H.B., Zhang, Q., Gong, J.Y., Liu, S.J., Yu, S.H., 2009. Hierarchical $FeWO_4$ microcrystals: solvothermal synthesis and their photocatalytic and magnetic properties. Inorg. Chem. 48, 1082–1090.

Zou, C., Zhong, J., Li, S., Wang, H., Wang, J., Yan, B., Du, Y., 2017. Fabrication of reduced graphene oxide-bimetallic PdAu nanocomposites for the electrochemical determination of ascorbic acid, dopamine, uric acid and rutin. J. Electroanal. Chem. 805, 110–119.